



ESCRT-III induces phase separation in model membranes prior to budding and causes invagination of the liquid-ordered phase

Yunuen Avalos-Padilla^{a,b,*}, Vasil N. Georgiev^a, Rumiana Dimova^{a,*}

^a Department of Theory and Bio-Systems, Max Planck Institute of Colloids and Interfaces, Science Park Golm, 14424 Potsdam, Germany

^b Nanomalaria Group, Institute for Bioengineering of Catalonia (IBEC), The Barcelona Institute of Science and Technology, Baldiri Reixac 10-12, ES-08028 Barcelona, Spain

ARTICLE INFO

Keywords:

ESCRT-III
Phase separation
Lipid domains
GUVs
Ternary mixtures
Membrane fission
Microcompartments

ABSTRACT

Membrane fission triggered by the endosomal sorting complex required for transport (ESCRT) is an important process observed in several pathogenic and non-pathogenic cellular events. From a synthetic-biology viewpoint, ESCRT proteins represent an interesting machinery for the construction of cell mimetic sub-compartments produced by fission. Since their discovery, the studies on ESCRT-III-mediated action, have mainly focused on protein dynamics, ignoring the role of lipid organization and membrane phase state. Recently, it has been suggested that membrane buds formed by the action of ESCRT-III are generated from transient microdomains in endosomal membranes. However, the interplay between membrane domain formation and ESCRT remodeling pathways has not been investigated. Here, giant unilamellar vesicles made of ternary lipid mixtures, either homogeneous in phase or exhibiting liquid-ordered/liquid-disordered phase coexistence, were employed as a model membrane system. These vesicles were incubated with purified recombinant ESCRT-III proteins from the parasite *Entamoeba histolytica*. In homogeneous membranes, we observe that EhVps32 can trigger domain formation while EhVps20 preferentially co-localizes in the liquid disordered phase. The addition of EhVps24 appears to induce the formation of intraluminal vesicles produced from the liquid-ordered phase. In phase separated membranes, the intraluminal vesicles are also generated from the liquid-ordered phase and presumably emerge from the phase boundary region. Our findings reinforce the hypothesis that ESCRT-mediated remodeling depends on the membrane phase state. Furthermore, the obtained results point to a potential synthetic biology approach for establishing eukaryotic mimics of artificial cells with microcompartments of specific membrane composition, which can also differ from that of the mother vesicle.

1. Introduction

Because of their fluid nature, cellular membranes are highly dynamic and able to adopt different shapes [1]. Processes in cells that involve a number of morphological and topological transitions in the membrane, including tubulation, budding and fission, require the generation of membrane curvature [2]. Among these processes, membrane fission represents an important step for many essential cellular functions including cytokinesis, endocytosis and membrane trafficking. Fission can be controlled by one or several active mechanisms (i.e. associated with energy consumption like in processes driven by dynamin or actin) or passive mechanisms (i.e. resulting from mechanical perturbation, membrane insertions, lipid domain formation and protein crowding

[3].

Passive mechanisms are of special interest as they merely rely on the reorganization of lipids and proteins that lead to membrane neck constriction and scission without the use of energy [3]. In addition, they represent an attractive route of establishing minimalistic approaches in synthetic biology aiming to reconstitute cell division (with a minimal divisome), see e.g. [4,5], or achieve microcompartment architectures either mimicking cells or for building artificial membrane-bound microsystems for achieving multistep reactions or drug release, see e.g. [6].

Giant unilamellar vesicles (GUVs) [7–11] have served as a convenient model membrane system in the study of passive mechanisms as they are easily accessible under a conventional microscope due to their

* Corresponding authors.

E-mail addresses: yavalos@ibecbarcelona.eu (Y. Avalos-Padilla), Rumiana.Dimova@mpikg.mpg.de (R. Dimova).

¹ Present address: Barcelona Institute for Global Health (ISGlobal, Hospital Clínic-Universitat de Barcelona), Rosselló 149-153, ES-08036 Barcelona, Spain.

large sizes. Passive membrane fission in this model is triggered by different mechanisms. For instance, one approach relies on mechanical perturbation applied using microfluidic strategy [12]. Another example is based on protein adsorption at low coverage via the modulation of the membrane spontaneous curvature and vesicle volume [13]. Highly crowded protein coverage, can also modulate membrane transformations and trigger fission [14]. An alternative approach involves the insertion of long-chain amphiphiles such as lysophosphatidylcholine [15] whereby fission of phase-separated vesicles, triggered by these compounds, occurs in the liquid-ordered phase [16].

Phase separation in lipid membranes is governed by chemical and architectural features of the constituting molecules [17]. Microscopic domain formation in model membrane systems is easy to establish, while in living cells such phase separation has been observed only rarely [18] and a few studies have shown presence of domains at the nanometer scale [19–23]; for a review on recent advances see [24]. Different *in vitro* studies have demonstrated that membrane domains can promote segregation and crowding by either incorporating or excluding proteins, which limits the lateral diffusion in the membrane and controls protein-protein and protein-lipid interactions [25,26]. Moreover, these specialized regions possess different physical properties characterized by the presence of line tension in their boundaries, which can trigger budding as theoretically predicted [27–29] and experimentally observed [30]. In this scenario, when the line tension changes and a membrane neck is present, the length of the domain boundary tends to shrink and can lead to membrane fission [31].

The endosomal sorting complex required for transport (ESCRT) machinery participates in different important cellular fission events including the formation of multivesicular bodies [32], cytokinesis [33,34], virus budding [35], exosome biogenesis [36] and neuron pruning [37] among others; see review in [38]. In all of these processes, the nascent vesicle buds away from the cytoplasm, a budding direction opposite to that observed in clathrin and COPI/II coated vesicles, as reviewed in [39]. In general, the ESCRT machinery is well conserved across the eukaryotic lineage and consists of ESCRT-0, ESCRT-I, ESCRT-II and ESCRT-III complexes [40]. Among these complexes, ESCRT-III (formed by Vps2, Vps20, Vps24 and Vps32) has shown to be responsible for vesicle scission in the majority of the ESCRT-related events [38]. In yeast, Snf7/Vps32, Vps24 and Vps2 (CHMP4, CHMP3 and CHMP2 in humans, respectively) seem to represent the minimal core for ESCRT-III function [41]. However, non-Opisthokonta organisms may exhibit alterations in this “minimal” set of proteins probably due to evolutionary reasons [40]. This is the case of the protozoan parasite *Entamoeba histolytica* in which the minimal core for ESCRT-III action is formed by EhVps20, EhVps32 and EhVps24 [42]. In this system, the main difference consists in the inability of EhVps32 to bind directly to the membrane in the absence of EhVps20 or other upstream activating factors [42]. However, the two other proteins appear to retain the same function as in higher eukaryotes. The recruitment of ESCRT-III to the site where scission occurs is carried out by the early acting factors: ESCRT-I/II for vesicle biogenesis [32] or Alix (Alg2-interacting protein X) for cytokinesis [33]. It is generally accepted that the ESCRT-III sub-complex forms an oligomeric array that interacts with the deformed membrane. This protein array suffers continuous rearrangements triggered by other ESCRT-III proteins like Vps2 and Vps24 [43] or by other ESCRT-III associated-proteins such as the AAA-ATPase Vps4 [44]. Finally, ESCRT-III-filaments are conferred with the elasticity necessary to close the neck of the nascent vesicle and produce membrane scission. In the majority of the work on model membranes, ATP has been employed to achieve ESCRT-III-mediated fission [44], even though it appears that both active and passive mechanisms are able to drive the process [45].

During the last years, several studies have attempted to reveal the nature of the underlying action of the ESCRT machinery and different mechanisms have been elucidated [46–51]. However, a consensus has not been established yet and most of the proposed models are incomplete because they ignore the biophysical properties of the deformed

membranes. Many studies suggest that there is more than one mechanistic scenario occurring in the ESCRT-driven processes and possibly involving intramembranous rearrangements [52–54]. For instance, it has been hypothesized that ESCRTs induce lipid cluster formation, which gives rise to a line tension at the domain boundaries thus providing the energetic driving force for ESCRT-mediated budding [55]. In accordance, other studies have shown that ESCRT-II can induce lateral lipid phase separation in supported lipid bilayers [56], although the line tensions generated by this process were not sufficient to drive budding [56]. Moreover, studies performed in worms [57] and in plants [58] showed that individual buds formed under the ESCRT influence are concatenated (i.e. interconnected like in a pearl-chain necklace), suggesting that they form continuously from stable microdomains. Supporting these studies, transient waves of ESCRT-III recruitment in endosomes of HeLa cells coupled with bud formation at the same microdomain have been observed [59]. Nevertheless, how lipid domain formation can influence the budding and scission triggered by ESCRT proteins has not been elucidated.

Model lipid membranes of ternary lipid mixtures have been widely used as a minimal system to investigate equilibrium dynamics of micromimetic sized lipid domains, as they exhibit spontaneous demixing into two defined liquid phases following thermodynamic principles as reviewed in [60,61]. The biomimetic model of giant vesicles [7–11] have served as a convenient model system to study passive fission mechanisms and the nature of the ESCRT-triggered reactions [42,62,63]. Moreover, it is possible to recreate liquid-liquid phase separation within GUV membranes that leads to the formation of large-scale lateral domains [64–67] thus possibly mimicking the formation of lipid domains in cells [68,69], even though the order and packing in the model and cell membranes might differ [70]. These domains exhibit different chemical characteristics, one of them is a relatively packed, ordered phase, enriched in saturated lipid species and cholesterol (called the liquid ordered, Lo phase), and the other one is a fluid, disordered phase comprising mainly unsaturated lipids (termed liquid disordered, Ld phase), see e.g. [71,72]. In general, Lo domains are employed as a mimetic model of lipid rafts [72,73] which are thought to be functional platforms that regulate important cellular mechanisms as they can incorporate or exclude proteins [25,26,74–76].

Here, we employed giant vesicles of ternary composition and investigated the action of ESCRT-III proteins on the membrane phase state. For this, purified ESCRT-III recombinant proteins from the phagocytic parasite *E. histolytica* were used as a model system. The protein behavior was tested on GUVs composed of ternary lipid mixtures prone to phase separation and containing negatively charged lipids, which are necessary for the recruitment and activation of ESCRT-III components at the membrane [63,77]. We investigated how protein binding influences the phase state of the membrane, the preferential partitioning of the proteins to specific membrane domains and the composition of the ESCRT-III-generated intraluminal vesicles. Passive mechanisms of fission, i.e. not requiring energy input, are advantageous for establishing minimalistic systems of multicompartiment eukaryotic-like artificial cells or division mimetic, because of (i) the reduced number of components needed to reproduce the whole process of binding, invagination and fission, and (ii) overcoming the otherwise imposed constraints from exhausting the energy supply. Thus we questioned whether, based on a minimal ESCRT-III system, one can establish vesicle microcompartmentation, where the composition and mechanical properties of the subcompartment membrane can selectively differ from that of the mother vesicle.

2. Materials and methods

2.1. Expression and purification of recombinant proteins

Recombinant proteins from *E. histolytica* were purified as described previously [42,78]. Briefly, protein expression was induced by the

addition of 1 mM of isopropyl β -D-1-thiogalactopyranoside (IPTG) in previously transformed *Escherichia coli* BL21 cells, to produce the glutathione S-transferase (GST)-tagged proteins EhVps20t, EhVps32 and EhVps24. Purified proteins were dialyzed against the buffer for the PreScission protease enzyme (GE-healthcare, Freiburg, Germany) (50 mM Tris-HCl, pH 7.0, 150 mM NaCl, 1 mM EDTA, 1 mM dithiothreitol) and the GST-tags were removed for 4 h at 4 °C, according to the manufacturer instructions. GST-free monomers were applied to a Superdex 200 16/600 column (GE-healthcare, Freiburg, Germany) connected to an Äkta-Purifier FPLC (GE-healthcare, Freiburg, Germany) and separated in working buffer. The working buffer for all proteins was 25 mM Tris, 150 mM NaCl, pH = 7.4. The pooled Superdex 200 fractions were confirmed by sodium dodecyl sulfate-polyacrylamide gel electrophoresis (SDS-PAGE) stained with Coomassie Blue, aliquoted in small volumes and stored snap frozen in liquid nitrogen until use.

2.2. Labelling of EhVps20t

The purified EhVps20t was labelled using either Oregon green 488 (OG) (Molecular Probes-Thermo Fisher) or Alexa Fluor™ 647 (Alexa 647) (Molecular Probes-Thermo Fisher) following the manufacturer protocol to obtain OG488-EhVps20t or Alexa 647-EhVps20t, respectively. The labelling reaction was performed with the corresponding dyes functionalized with succinimidyl ester groups that covalently label the protein on primary amines to form a stable amide linkage. Briefly, purified proteins were dialyzed against 0.1 M sodium bicarbonate buffer, pH 8.3 and incubated with 50 μ l of reactive dye solution (prepared at a 10 mg/ml stock solution) for 6 h at 4 °C. The labelled and unlabelled proteins were separated by size exclusion chromatography with a Superdex 200 16/600 column (GE-healthcare, Freiburg, Germany) connected to an Äkta-Purifier FPLC (GE-healthcare, Freiburg, Germany). Based on our experience, labelling ESCRT-III proteins can reduce protein functionality, presumably due to conformational changes in the binding sites as previously observed with other proteins [79–81], making it necessary to increase protein concentration to achieve a similar effect. Therefore, in all cases, a 1:4 ratio of labelled: unlabelled proteins was used to maintain protein activity.

2.3. Preparation of giant unilamellar vesicles

The lipids 1,2-dioleoyl-sn-glycero-3-phospho-(1'-rac-glycerol) (DOPG), egg sphingomyelin (eSM), cholesterol (Chol), 1-palmitoyl-2-oleoyl-sn-glycero-3-phosphocholine (POPC), 1-palmitoyl-2-oleoyl-sn-glycero-3-phosphocholine (POPS) and 2-dioleoyl-sn-glycero-3-phospho-(1'-myo-inositol-3'-phosphate) (PI(3)P) were purchased from Avanti Polar Lipids (Alabaster, IL). Lipid stock solutions at 4 mM of different lipid compositions and including 0.3 mol% DiI_{C18} (1,1'-dioctadecyl-3,3',3'-tetramethylindocarbocyanine perchlorate, Molecular Probes) were prepared. The lipid ratios used to measure ESCRT-III activity were 10:3:87 (POPS:PI(3)P:POPC), 20:80 (POPS:POPC) and 20:80 (DOPG:POPC). The ternary mixtures in which we explored the effect of membrane phase state, were set to the following DOPG:eSM:Chol:DiI_{C18} mole ratios: 10:64.7:25:0.3 (denoted as 10:65:25 in the main text for simplicity) for homogeneous vesicles, and 20:49.7:30:0.3 (referred to as 20:50:30) for phase separated GUVs. For double labelled phase-separated GUVs, the mole ratio used was 20:48.95:30:0.3:0.75 DOPG:eSM:Chol:DiI_{C18}:DSPE-PEG2000-CF where the second dye was 1,2-distearoyl-sn-glycero-3-phosphoethanolamine-N-[poly(ethylene glycol) 2000-N'-carboxyfluorescein] (Molecular Probes). No difference in the area fraction of the domains was detected compared to the vesicles labelled only with DiI_{C18} (note that relatively low laser intensity and sensitive hybrid detectors were used for imaging to avoid photo-oxidation [82,83]). GUVs were grown using the electroformation method [84]. Briefly, 10 μ l of the different lipid stock solutions prepared in chloroform were spread on indium tin oxide (ITO) coated glasses. The excess of chloroform was eliminated under vacuum at room temperature

(RT) for 1 h. Then, the glasses were assembled with a 2 mm-thick Teflon spacer between them to form the electroformation chamber, which was filled with a 600 mM sucrose solution that matched the osmolarity of the buffer containing the proteins (~650 mOsm). Finally, an electric AC-field (1.6 V, 10 Hz) was applied for 1 h at 60 °C, i.e. above the melting temperature of eSM to ensure miscibility. GUVs were collected and cooled to room temperature before use. In the case of the ternary mixtures, experiments were performed on more than 10 different preparations and in all cases more than 95% of the vesicles were homogeneous for the 10:65:25 mixture and phase separated for the 20:60:20 mixture.

2.4. ESCRT-III reconstitution on GUVs and imaging

For reconstitution experiments, GUVs were diluted 1:1 to the 2-fold protein buffer (50 mM Tris, 300 mM NaCl, pH = 7.4) and subsequently incubated at RT with final concentrations of 125 nM of either OG488-EhVps20t or Alexa 647-EhVps20t (labelled:unlabelled 1:4 ratio), 600 nM of EhVps32 and 200 nM of EhVps24 as indicated in the figures captions. In some cases, we included 200 nM of the soluble marker GFP (28 kDa, Thermo Fisher) after EhVps20t addition.

All images were acquired by confocal microscopy on a Leica TCS SP8 confocal microscope (Mannheim, Germany) equipped with a 63 \times objective of 1.2 NA. DiI_{C18} was excited with a diode-pumped solid-state laser at 561 nm (10% intensity), Alexa 647 with a helium-neon laser at 633 nm (13% intensity), and OG with the 488 nm line of an Argon laser (8% intensity). To avoid crosstalk between the different fluorescence signals, sequential line scanning was performed. For the DiI_{C18} dye, the fluorescence signal was collected in the ranges of 580–650 nm, for Alexa 647 signal was collected in the ranges of 670–740 nm and the fluorescence signal of OG and DSPE-PEG2000-CF was collected between 495 nm and 530 nm. For acquisition, we performed bidirectional scanning, the speed was maintained at 700 Hz and the pinhole size was set to 1 Airy unit. The gain and laser intensity was maintained fixed for all experiments. In all conditions, the GUVs were examined under phase contrast microscopy. During the time of acquisition (10 min average), no changes in the domain area size were observed suggesting no photo-oxidation [82,83]. Because of the difference in the refractive indexes of the GUV-enclosed and the surrounding media, the vesicles appear dark with a brighter halo. Contrary to surface domains on the GUV, intraluminal buds and vesicles, which have formed under the action of the ESCRT proteins, appear as brighter spots inside the GUV as they encapsulate external media. In this way, they could be distinguished from membrane domains of internal defects (defects are occasionally present inside GUVs and result from the preparation protocol). In all cases, conclusions about the presence of intraluminal buds and vesicles and/or membrane domains were based on both fluorescence and phase contrast imaging. For this purpose, 3D scans of the vesicles were acquired and scanning was performed at lower resolution to allow fast imaging of the whole or half vesicle (to avoid smearing resulting from displacement of intraluminal structures or the whole vesicle due to convection or flow in the microfluidic channels). Note that for scanning of a whole vesicle of typical diameter of 30 μ m in our conditions takes 2 min approximately.

2.5. Microfluidic chamber

A microfluidic device was used to trap GUVs in order to assess the effect of ESCRT proteins on phase separated vesicles and to observe the domain where the budding occurs upon introducing the protein or washing away the excess. The device also allows for following individual vesicles throughout the whole process, which represents an advantage over bulk experiments where the history of the observed vesicles (e.g. a priori presence of intraluminal vesicles) is unknown. The design and fabrication of the device has been detailed elsewhere [85]. The PDMS chips were produced using standard soft photolithography and

assembled by bonding the PDMS chip to a glass coverslip, see [85] for detailed procedures. The chips were generously provided to us by T. Robinson. Before the experiment, the devices were coated with 2% BSA (bovine serum albumin, Sigma Aldrich) dissolved in the protein buffer (25 mM Tris, 150 mM NaCl, pH = 7.4). Then, 100 μ l of phase separated GUVs were loaded into the device at a flow rate of 10 μ l/min using a syringe pump (neMESYS, cetoni) to control the flow. To avoid losing of captured vesicles in the following steps, the flow rate was lowered to 0.1 μ l/min. As a control to test whether protein-free buffers induce any morphological changes, the GUV buffer was fully exchanged with 100 μ l of the isotonic protein buffer. Afterwards, EhVps20t was added to the chamber to yield a final concentration of 125 nM, then EhVps32 (600 nM) and EhVps24 (200 nM) were added in that order while maintaining the flow rate in the whole experiment. Similarly, phase separated GUVs were incubated with four rounds of buffer as a negative control.

3. Results

3.1. EhVps32 induces phase separation in raft-like GUVs

Previously, we have shown that the core domain of Vps20 from *E. histolytica*, EhVps20t, is able to bind to the membrane of homogeneous negatively charged GUVs and together with EhVps32 and EhVps24 generate intraluminal vesicles [42]. We have also resolved the individual role of the latter two proteins. Namely, EhVps32 binds to EhVps20t and generates inward buds, the fission of which is then triggered by EhVps24 in the absence of ATP. Moreover, we have observed that the buds formed after the addition of EhVps20 and EhVps32 were similar in size [42]. We speculated that the uniform bud size is a result of phase separation of the adsorbed protein layer into a EhVps32-rich and a EhVps32-poor domains and that the EhVps32-rich domains have a significant spontaneous curvature that determines the bud size [86].

In order to explore the protein effect on the membrane phase state, we studied the behavior of recombinant ESCRT-III proteins in multi-component sphingomyelin-containing GUVs. The vesicles were composed of a ternary mixture of the neutral high-melting temperature lipid egg sphingomyelin (eSM), the negatively charged unsaturated lipid dioleoylphosphatidylglycerol (DOPG) and cholesterol (Chol). The phase diagram of this mixture has been explored previously and, for certain compositions, phase separation and domain formation has been observed in giant vesicles [87]. The presence of negatively charged lipids in the membrane is a prerequisite for ensuring electrostatic binding of the exposed basic surfaces present in ESCRT-III proteins as demonstrated in studies on ESCRT-III polymerization in synthetic membranes [41,52]. Some ESCRT-III proteins have been demonstrated to exhibit specific affinity to certain anionic lipids, especially PIP species

[88–90]. However, in the case of *E. histolytica* -ESCRT-III subunits, we do not observe preferential activity to a certain anionic lipid specie as long as the total net charge on the membrane is maintained (Fig. S1). Based on previous work investigating asymmetric sucrose/salt conditions across the bilayer and their effect on the phase state of these membranes [91,92] and because of to lack of other phase diagrams with charged lipids, we selected a DOPG-based composition (DOPG:eSM:Chol 10:65:25, see Materials and Methods) which does not exhibit microscopic phase separation and tested that this behavior is preserved in our buffer conditions and in the absence of the ESCRT proteins (Fig. 1). The lipid mixture included a small fraction of DiI_{C18} dye as a marker of Ld domains [93]. Note that the image of the homogeneous vesicle in Fig. 1 appears brighter at the poles not because of phase separation but because of dye polarization effects, see e.g. [94]. For tests with domains of the liquid ordered phase we occasionally used DSPE-PEG2000-CF to visualize them (see Materials and Methods and left image in Fig. 1). However, because of the bulky part of the headgroup of this lipid dye, we avoided as much as possible using it in the presence of the proteins. Nevertheless, it is important to mention that when phase separated GUVs incorporating this dye were incubated with different rounds of protein buffer, the domain area fraction remained unaltered.

Upon incubation of the homogeneous GUVs (DOPG:eSM:Chol 10:65:25) with 125 nM of EhVps20t, the protein bound to the membrane and did not affect the membrane homogeneity (Fig. 2a, first row of images). The binding was monitored via fluorescence signal from Oregon Green labelled protein (OG-EhVps20t) added at a fraction of 1:4 labelled to unlabelled protein. The labelled protein showed homogeneous fluorescence over the whole vesicle examined with 3D confocal scanning. However, after EhVps32 was included in the mixture, an evident phase separation occurred. Interestingly, EhVps20t (as monitored with OG-EhVps20t) co-localized with the lipid dye (DiI_{C18}), thus apparently relocating to round Ld-like membrane domains (see Fig. 2a, second row of images, and Fig. S2 in the Supporting Information). The domains were fluid as evidenced from coalescence leading to the formation of larger domains with time (images of other vesicles immediately after incubation with the proteins exhibiting smaller domains, which have not yet coalesced are shown in Fig. S3). Their displacement along the vesicle surface is an evidence that the dye-depleted phase is fluid too, presumably liquid ordered as DiI_{C18} typically marks Ld domains [93]. The vesicles remain intact upon the addition of the proteins as suggested by the preserved phase contrast enhanced by the in/out sugar/salt asymmetry. Note that the inner membrane leaflet, which was not exposed to the proteins, appears to be phase-separated as well, as no significant fluorescence in the membrane was observed around the DiI_{C18}-rich domains, presumably indicating domain registration [95]. Phase separation was observed in an EhVps32 concentration-dependent

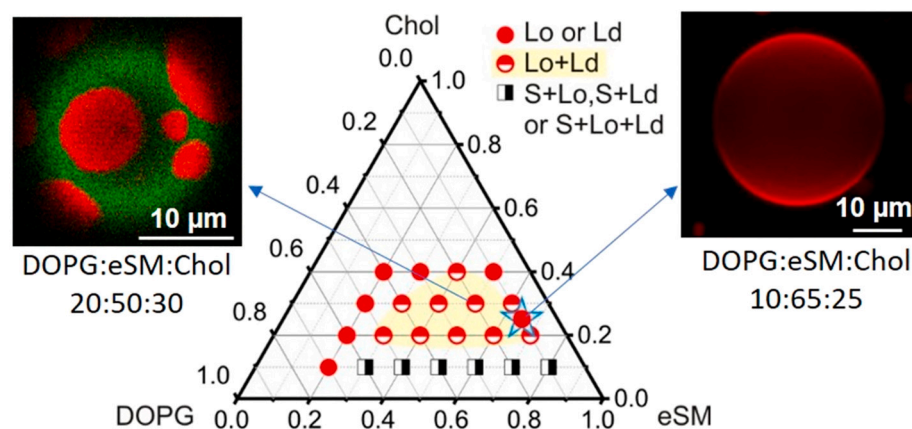


Fig. 1. Phase diagram and explored lipid mixtures. The regions of homogeneous membrane (solid circles), liquid-ordered and liquid disordered phase coexistence (half-filled circles) and solid and fluid coexistence (half-filled black squares) are indicated in the Gibbs triangle of DOPG:eSM:Chol mixtures consistent with data reported in [91]. The liquid-liquid phase coexistence region is highlighted in yellow. In this work, we selected two membrane compositions to explore – a homogenous one (indicated with a star), close to the binodal, and a phase separated one exhibiting coexistence of liquid ordered and liquid disordered domains. Arrows point to representative images of the mixtures employed in this work. GUVs were labelled with DSPE-PEG2000-CF (green, 0.75 mol%) which partitions mostly in the Lo phase and DiI_{C18} (red, 0.3 mol%) labelling the Ld phase. (For interpretation of the references to color in this figure legend, the reader is referred to the web version of this article.)

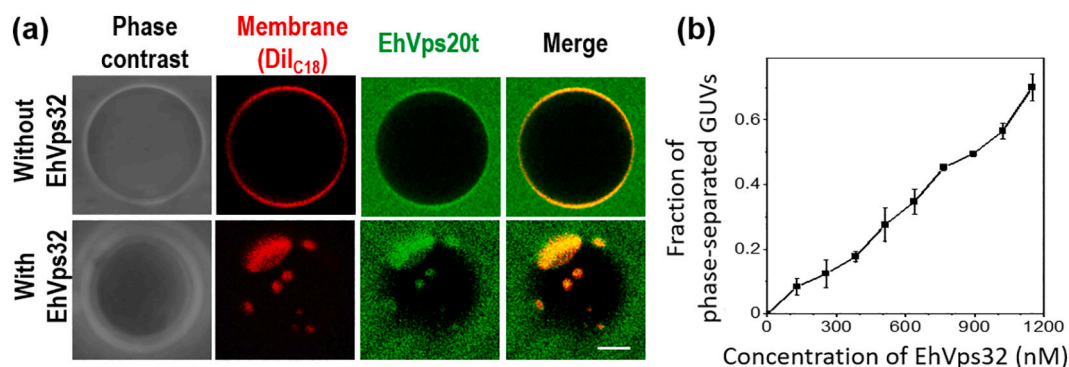


Fig. 2. EhVps32 induces phase separation in initially homogeneous membranes. (a) Homogeneous GUVs (DOPG:eSM:Chol 10:65:25, and 0.3 mol% DiI_{C18}, false color red) incubated for 10 min at room temperature with 125 nM of a mixture of 1:4 labelled:unlabelled EhVps20t, false color green (top row) or in combination with 600 nM EhVps32 (bottom row of images showing a cross section in the upper part of the vesicle for better visualization of the curved vesicle surface with domains; for other cross sections at different height through the vesicle, see Fig. S2 in the Supporting information). Scale bars correspond to 10 μ m. (b) Fraction of GUVs exhibiting phase separation as a function of EhVps32 concentration. Experiments were done with the same GUV batch for comparability. Each experiment was repeated at least three times with different batches of GUVs. On the average, 20 random vesicles of appropriate size (typically above 15 μ m in diameter) were examined for phase separation in each batch. (For interpretation of the references to color in this figure legend, the reader is referred to the web version of this article.)

manner (Fig. 2b). On the average 20 GUVs with diameters in the range 15–30 μ m were examined with 3D confocal scans or epifluorescence for presence of domains. At EhVps32 concentrations around 800 nM, approximately half of the vesicles appeared phase separated. The vesicle area fraction occupied by the Lo phase did not appear to change as a function of protein concentration (Fig. S3).

3.2. Intraluminal vesicles are generated from the liquid-ordered (Lo) phase

Under the explored concentration conditions, the binding of EhVps32 is supposed to induce inward buds in the vesicles [42]. Membranes with Ld composition are, in general, softer than Lo membranes [96,97]. Thus, the less rigid Ld membrane is expected to favor invagination as it imposes lower energy barrier. However, we could not detect the formation of nascent buds from the Ld phase. In our working conditions, the Lo phase was not labelled (as EhVps20t was) and we speculated that the detection of Lo buds is hindered because the liquid-ordered phase is not detected (black) in confocal images. Tests with DSPE-PEG2000-CF did not show strong preference of this dye to the Lo phase, which hinders distinction of ESCRT-generated intraluminal buds or vesicles from internal vesicle defects. To overcome this imaging difficulty, and to visualize bud formation, we incubated the GUVs with unlabelled EhVps20t and EhVps32 at the concentration mentioned above and introduced soluble GFP protein (28 kDa) in the solution immediately after EhVps20t addition. Therefore, the newly EhVps32-generated inward buds would contain this marker allowing us to follow their formation. In addition, membrane defects as intraluminal vesicles present in the GUVs before the addition of the proteins could be excluded, as they would not contain GFP. In accordance with Fig. 2a, phase separation was observed after EhVps32 addition however, no buds could be detected (Fig. 3a). The reason for this behavior could be either that no buds were formed, or that the fluorescence from GFP in the buds is diffuse and weak (due to the small bud size and high mobility) and poorly detectable because of the strong adjacent fluorescence signal from GFP present outside the vesicle. We speculated that if it were the latter, detaching the buds from the vesicle membrane, thus forming intraluminal vesicles (ILVs) in the GUV interior (thus creating higher contrast), would help visualizing them by means of the GFP signal. In our previous study using *E. histolytica* ESCRT-III proteins, we showed that intraluminal buds are detached from the mother vesicle after EhVps24 addition. Therefore, this third protein was included to the current system and we observed that, once unlabelled EhVps24 (200 nM) was added, GFP-containing ILVs could be detected in the GUV

interior (Fig. 3b, arrows, see also Fig. S4 and Movie S1 in the Supporting information). The experiments were replicated twice on vesicle batches from different preparations. The ILVs appeared to have homogeneous sizes over the whole vesicle population with diameters roughly in the range 1–2.8 μ m (precise determination was not possible due to the very diffuse bulk GFP signal in the ILVs, which decays close to the ILV surface). Nevertheless, the observed GFP-loaded ILVs excluded the DiI_{C18} dye confirming that the action of EhVps32 and EhVps24 is fully restricted to the Lo phase. Note that the weak signal in the DiI_{C18} channel (merged image in Fig. 3b) results from inward tubes occasionally present in the GUVs before the addition of the proteins. Presumably, these tubes originate from negative membrane spontaneous curvature imposed by the buffer asymmetry across the membrane as recently demonstrated [98]. The signal from these tubes does not overlay with that from the ILVs.

Finally, we also probed the effect of the ESCRT proteins on phase-separated vesicles (see the vesicle composition indicated in Figs. 1 and 3D GUV images in Fig. 4). In this case, we included the dye DSPE-PEG2000-CF to visualize the Lo phase. First, we evaluated the binding of EhVps20t in this membrane composition using the Alexa 647-labelled protein. Fig. 4a shows that EhVps20t retained its localization in the Ld phase as demonstrated by the colocalization of the signal of Alexa 647 and the dye DiI_{C18}. However, our previous experience showed that labelling of proteins compromises their activity, presumably due to conformational changes in the binding sites as previously observed with other proteins [79–81]. Thus, the subsequent experiments were carried out with unlabelled proteins. In this approach, microfluidic technology was used to follow the effect of ESCRT proteins on a single vesicle while removing the excess of the protein in the surrounding buffer to avoid unspecific effects due to protein excess. The vesicles were loaded in the microfluidic chip and immobilized by a gentle flow pressing them against the posts of the device. As a control, we probed whether addition of protein-free buffer induces morphological changes in the vesicle. None were observed and the phase separation in the membrane was preserved, see first image in Fig. 4b. Then, the incubation of phase-separated GUVs with EhVps20t (125 nM), EhVps32 (600 nM) and EhVps24 (200 nM) added sequentially in that order, led to the expected production of ILVs whose membrane is only labelled with DSPE-PEG2000-CF and had excluded the DiI_{C18} dye, indicating that the newly formed vesicles were generated from the Lo phase and thus confirming our previous observations. In these experiments, the incubation time was longer (~1 h) compared to that employed in the bulk batch experiments (~10 min). As a result, the smaller domains have coalesced leading to two large domains of Ld and Lo phase. The

experiments were replicated twice on different vesicle preparations (see also Movies S2 and S3 exemplifying vesicles from two different samples). The number of observed ILVs was in general lower compared to that detected in free-standing GUVs (as in Fig. 3 and previously in [42]). The main reasons for this observation is the limiting dimensions in height of the microfluidic channel ($\sim 20 \mu\text{m}$), which causes the larger vesicles to be squeezed inducing tension on the membrane and reducing the excess area available for invagination and formation of ILVs.

We attempted to resolve the vesicle area change as well as the change in the Lo/Ld area ratio resulting from the generation of ILVs from the Lo phase. However, this proved not feasible, because of the large error associated with estimating the vesicle area from confocal scans of vesicles trapped in the microfluidic channels, see [99], and the very small area of the ILVs.

4. Discussion

Over the last decades, the ESCRT machinery has gained a lot of attention due to its participation in important cellular processes and the unique budding topology it triggers. However, it has been difficult to generate a model that explains its mechanism of action, probably because of the high complexity of the protein-membrane interactions. In particular, the ESCRT-III complex involved in all ESCRT-related fission processes has been extensively studied. It has been shown that ESCRT-III assemblies are remodelled by Vps4 and that this reorganization is responsible for membrane scission [100]. Therefore, it is known that ESCRT-III proteins form a membrane-interacting oligomeric filament that is believed to operate the membrane remodeling event resulting in scission [44]. These findings have been reinforced by studies showing that budding and scission *in vivo* occurs only when sufficient Vps4 is recruited to the endosome [100]. It has been recently demonstrated that ALIX-mediated ESCRT-III recruitment is enhanced at lower membrane tension leading to membrane deformation coupled to ESCRT-III polymerization [101]. In addition, purified ESCRT-III components have been shown to produce budding in a passive manner in biomimetic models such as GUVs [42,62,63,102]. Alternatively, it has been proposed that ESCRT proteins can modify the local lipid composition [103] and induce lipid cluster formation where the main shaping force provided by the line tension at the lipid boundaries facilitates budding [55]. However, the formation of these lipid clusters preceding ESCRT-III mediated

budding has not been observed in living cells.

We used the biomimetic model of GUVs to study lipid domain formation during ESCRT-III action. Our results show that EhVps32 can trigger liquid-liquid phase separation in homogeneous GUVs composed of ternary mixtures (DOPG:eSM:Chol) in accordance with the previously reported effect of ESCRT-II on supported lipid bilayers [56]. Moreover, we observe that EhVps20t binds homogeneously to the membrane of these GUVs preserving the one-phase state of the membrane. Therefore, we conclude that liquid-liquid phase separation is triggered exclusively by EhVps32. Previous work suggests that EhVps32 and its activated version EhVps32(1-165) on their own do not bind to the membrane of negatively charged GUVs in the absence of EhVps20t [42]. Presumably, EhVps20t and EhVps32 act in tandem and their binding to each other alters the functionality (or structure) of EhVps32, which starts to assemble on the membrane surface and adsorbs to the negatively charged membrane. This behavior is similar to that of its human homologue CHMB4B, which adsorbs on negatively charged supported lipid bilayers [56,90]. Our finding that, in addition to adsorption, EhVps32 triggers phase separation could be explained by the ability of EhVps20t and EhVps32 to bind and potentially condense negatively charged lipids. This results in a local increase of their concentration and explains the appearance of negatively charged Ld domains as imaged by the fluorescent dye (note that DiI_{C18} does not exhibit a negative charge and its distribution should not be affected by interaction with the proteins).

Our studies were performed at relatively high protein concentration, which might raise concerns regarding the effect on the membrane curvature or phase state (as shown previously, different species in the solution can affect the membrane phase state [76,91,92] or induce sterically-imposed curvature as shown e.g. in [14]). Considering only EhVps20t, as this is the only protein directly interacting with the membrane, we estimate the protein-to-lipid molar ratio to be around 1/90 for mixing in the bulk (only the lipid in the external membrane leaflet was taken in account). However, this ratio is substantially overestimated because not all of the protein binds to the membrane as seen from the green signal of unbound protein around the vesicles in Fig. 2 (note that in the microfluidic experiments the excess unbound proteins are washed away and thus the protein-to lipid ratio is much lower). We believe that the relatively high protein concentration explored here does not affect our conclusions as (i) washing away the excess (unbound) protein in the microfluidic experiments does not appear to change the membrane

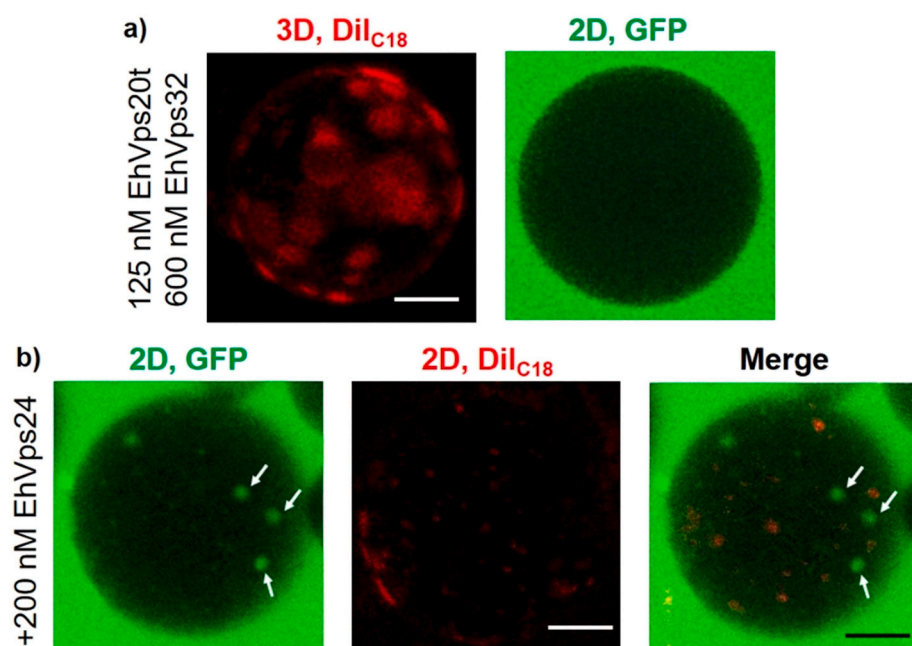


Fig. 3. Intraluminal vesicles form from the liquid ordered phase. GUVs (DOPG:eSM:Chol 10:65:25) labelled with DiI_{C18} (0.3 mol%, red) were subsequently incubated with unlabelled 125 nM EhVps20t, 200 nM of the soluble marker GFP and 600 nM EhVps32 in that order at room temperature. (a) 3D reconstruction of the total projection of the DiI_{C18} channel showing the Ld membrane domains (in red) on the surface of a GUV after EhVps20t, GFP and EhVps32 addition. On the right, cross section of the same GUV showing the GFP signal and absence of ILVs. (b) Cross sections of the GUV after the subsequent addition of 200 nM of EhVps24 to the above mixture. Arrows show GFP-loaded intraluminal vesicles (ILVs) that are not colocalizing with signal from DiI_{C18} labelling the Ld phase suggesting that they are produced from the Lo phase. More ILVs are seen on the additional cross sections provided in Fig. S4. Scale bars: 10 μm . (For interpretation of the references to color in this figure legend, the reader is referred to the web version of this article.)

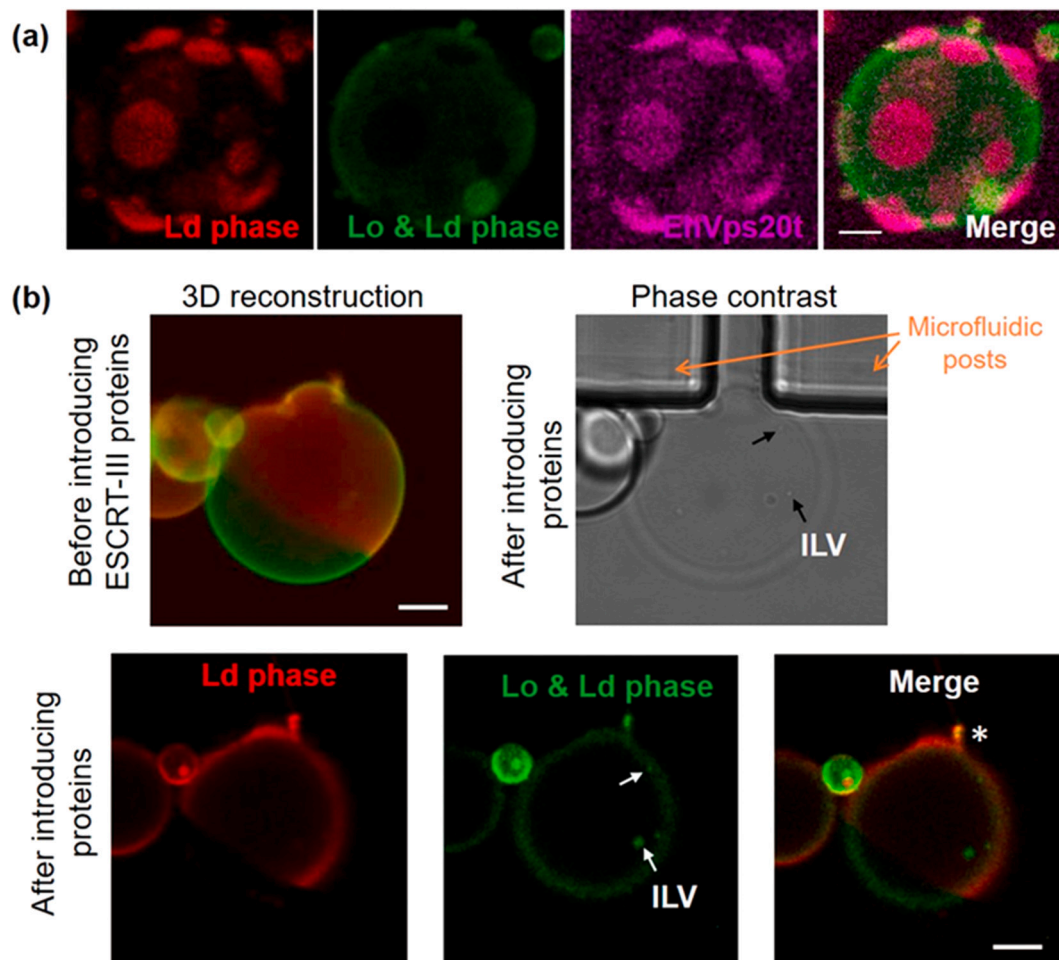


Fig. 4. ESCRT proteins induce budding and ILV formation from Lo domains. Initially phase separated GUVs (DOPG:eSM:Chol 20:50:30, 0.3 mol% DiI_{C18}, false color red and 0.75 mol% DSPE-PEG2000-CF, false color green) were loaded into a microfluidic device and incubated at room temperature with (a) 125 nM 1:4 (labelled: unlabelled) Alexa 647-EhVps20t to confirm that EhVps20t colocalizes with the Lo phase or (b) a mixture of 125 nM EhVps20t, 600 nM EhVps32 and 200 nM EhVps24 to resolve the phase of the generated ILVs. The latter are detected under phase contrast as small bright spots and in the confocal cross-sections as green specks (lacking DiI_{C18} signal as Ld marker) confirming that they are generated from the Lo phase. Other cross sections from the same vesicle provided in Fig. S5 show the presence of other ILVs located at different heights inside the vesicle. Note also the preserved partitioning of DiI_{C18} as Ld marker in the absence and presence of the proteins. The vesicle is deformed in the upper part by the microfluidic posts because of the applied flow to prevent it from drifting away. Asterisk shows a fragment of a small vesicle ruptured at the microfluidic post. Scale bars correspond to 10 μ m. (For interpretation of the references to color in this figure legend, the reader is referred to the web version of this article.)

phase state (Fig. 4b), and (ii) there is no substantial change of the area fraction of the phases (Fig. S3). Furthermore, curvature induced effects as a result of protein crowding [14] act in the opposite direction and should have induced outward buds, which are not observed here. Occasionally, we do observe inward tubes in the vesicles, but not as a result of the addition of the proteins. They are presumably stabilized by small asymmetry in the charged lipid distribution during GUV electroformation or buffer asymmetry as shown previously [91,104].

Interestingly, contrary to studies on membranes in the absence of the third component (EhVps24) in the mixture [42], we were not able to detect inward bud formation. To test the speculation that buds form from the Lo phase, which was not labelled in our homogeneous vesicles (making the buds “invisible”), we added the soluble dye GFP to the solution after EhVps20t incubation. Again, we observed the formation of lipid domains when EhVps32 was included in the mixture, and only after EhVps24 addition, GFP-loaded intraluminal vesicles appeared (this time made visible by the GFP). In our system, the addition of EhVps24 can lead to changes in the polymer shape favoring inward budding as proposed before [56,105]. This is also supported by recent studies [106] showing that the assembly and interactions of ESCRT-III filaments can trigger buckling of the membrane of large unilamellar vesicles. Here,

EhVps24 can presumably constrict the EhVps32 polymers, which in turn produces ILVs in a process similar to that mediated by Vps4 *in vivo*. EhVps32 polymerization has been already observed *in vivo* [78] leading to extensive formation of buds or cellular protrusions upon over-expression of *pNeoEhVps32-HA* transfected trophozoites. Experiments on supported lipid bilayers also showed the spiral-like polymerization of Vps32 putting forward the hypothesis for the protrusion of EhVps32 polymers out of the membrane plane [54]. In our experiments, buds were formed from the Lo phase but EhVps32 polymerization should have initiated from the Ld phase where EhVps20t resides, which suggests that the bud formation originates from the Ld/Lo phase boundary. The co-localization of EhVps20t with Ld domains observed here could be explained by the truncation performed in the protein that leaves only the positively-charged core exposed. Hence, it is likely that this core binds to negatively charged lipids (in our case DOPG) which, in this type of ternary mixtures, are enriched in the Ld domain.

A possible mechanism of the action of the proteins corresponding to the observed events is proposed in Fig. 5. In summary, EhVps20t binds to the homogeneous multicomponent membrane without altering its homogeneous appearance (Fig. 2a). EhVps32 then binds to EhVps20t and (i) initiates Lo/Ld phase separation in the membrane presumably via

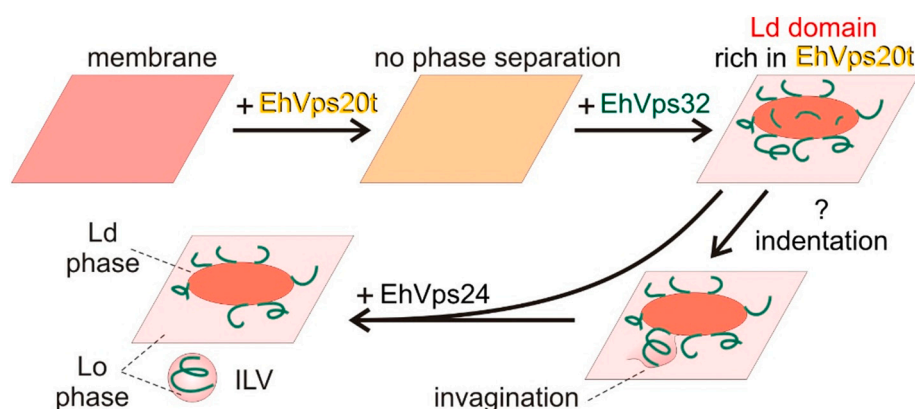


Fig. 5. Possible schematics of the action of ESCRT-III proteins in membranes prone to phase separation. EhVps32 adsorbs on membranes in the presence of EhVps20t and triggers phase separation with liquid disordered domains enriched in EhVps20t, but does not lead to detectable membrane buckling and bud formation. EhVps32 polymers (demonstrated previously in [43,52,54,78]) located at the Ld domain rim plausibly trigger small membrane indentation, i.e. buckling (not visible optically), in the surrounding Lo phase away from the EhVps20t-crowded Ld domain. Only in the presence of EhVps24, ILVs with membrane in the Lo phase are produced.

reducing the electrostatic repulsion, whereby colocalizing with the Ld phase (Fig. 2), and (ii) starts polymerizing into filamentous structures [43,52,54]. We hypothesize that these polymers, even though confined to and by the Ld domain boundaries, could protrude or stretch out into the surrounding Lo phase (plausibly also because the Ld one is overly saturated by EhVps20t) and even deform it producing inward indentation. This deformation must originate at the phase boundary in order to lead to the generation of ILVs with Lo phase membrane composition (Figs. 3 and 4). Only upon the addition of the third protein, EhVps24, which is known to induce changes in the polymer shape favoring inward budding, ILV formation initiates. Further interrogation, for example using Cryo EM, of the phase separated bilayers incubated with ESCRT-III proteins is necessary to unequivocally probe this.

Budding in GUVs is possible if excess area is available, i.e. at low membrane tension. Our observation is that the number of observed ILVs in the tense GUVs pressed into the microfluidic device is smaller (around 31 ± 9 ILVs) than in the less tense free-standing GUVs (47 ± 4). This is consistent with recent observations on tension-dependent ILV formation in living cells, where polymerization of ESCRT-III subunits (specifically CHPM4B, human homologue of EhVps32) causing membrane deformation was shown to be more pronounced at lower endosomal membrane tension [101].

Confining fission of phase-separated vesicles to the liquid-ordered phase as reported here is reminiscent of similar behavior observed upon the asymmetric insertion of amphiphiles (with a single long hydrocarbon chain) into vesicle membranes whereby fission was restricted to the liquid-ordered phase [16]. Fission in that case was not observed in vesicles belonging to the liquid-disordered phase. The authors explained the observed behavior considering the energetic contributions using the area difference elasticity model, in which the elastic energy of a GUV represents the sum of bending and relative monolayer stretching contributions [107]. The latter changes as the amphiphiles insert into the external leaflet of the vesicle membrane. Here, the condensing role of the EhVps20t-EhVps32 assembly on the outer charged membrane leaflet could act in a similar fashion to alter the membrane packing asymmetrically. Inaoka and Yamazaki speculated that because of the constraint for lipids to adopt all-trans configurations in the liquid-ordered phase, the packing perturbation in the Lo phase would be higher than in Ld domains, and could result in higher probability of the propagation of defects leading to fission [16]. A similar mechanism could play a role in the Lo-preferential fission triggered by ESCRT proteins as observed here.

Our results obtained on a minimalistic fission system consisting of only three proteins and in the absence of ATP are important for synthetic biology approaches targeting the construction of synthetic cells with functional compartments. Such systems represent a major step towards establishing the structural (compartmentalized) mimetic of eukaryotic cells. Previous studies employed a number of different approaches [108–111], the most efficient of which involves the use microfluidics on double emulsions for the preparation of ILVs in GUVs, i.e. nested vesicles

in vesicles or vesosomes. However, one drawback of this approach is the difficulty of protein reconstitution in such membranes as they originate from the assembly of monolayers at the oil-water interface of emulsion droplets. Presumably, the approach of generating micron-sized compartments (ILVs) in GUVs ensured by the three ESCRT proteins as introduced here can offer a path towards creating micro-compartmentalized synthetic cells, whereby the membrane composition of the compartments can be controlled by the composition of the starting vesicle.

5. Conclusion

Altogether, our results reinforce the idea that the mechanism of action of the ESCRT machinery is not only controlled by protein-protein interactions but also by lipid-protein and lipid-lipid interactions. It will be interesting if further studies explore the effect of lipid tail saturation, surface charge and membrane rigidity on the phase preference of the action of ESCRT proteins. For example, investigating membrane compositions in which the Lo phase has higher surface charge than the Ld phase would show whether the surface charge of membrane order has a stronger influence on the invagination process. Furthermore, to better mimic the direction of ESCRT-mediated remodeling of the plasma membrane, the proteins could be introduced in the intraluminal (cytosolic) side of the vesicle. For this, local microinjection of small volumes of protein solutions could be considered, which represents current direction of our work.

Supplementary data to this article can be found online at <https://doi.org/10.1016/j.bbmem.2021.183689>.

CRedit author contribution statement

This research was designed and coordinated by Y.A.-P. and R.D. Experiments were performed by Y.A.-P. and V.N.G. The manuscript was written by Y.A.-P. and R.D.

Declaration of competing interest

The authors declare that they have no known competing financial interests or personal relationships that could have appeared to influence the work reported in this paper.

Acknowledgments

Authors thank R. Seckler and S. Barbirz for kindly providing their facilities for protein purification. We acknowledge T. Robinson for the help with the microfluidic chips and T. Seeman for their preparation. This work is part of the MaxSynBio consortium, which is jointly funded by the Federal Ministry of Education and Research of Germany and the Max Planck Society.

References

- [1] F.M. Göni, The basic structure and dynamics of cell membranes: an update of the singer-nicolson model, *Biochim. Biophys. Acta Biomembr.* 2014 (1838) 1467–1476.
- [2] P. Bassereau, R. Jin, T. Baumgart, M. Deserno, R. Dimova, V.A. Frolov, P. V. Bashkurov, H. Grubmüller, R. Jahn, H.J. Risselada, L. Johannes, M.M. Kozlov, R. Lipowsky, T.J. Pucadyil, W.F. Zeno, J.C. Stachowiak, D. Stamou, A. Breuer, L. Lauritsen, C. Simon, C. Sykes, G.A. Voth, T.R. Weikl, The 2018 biomembrane curvature and remodeling roadmap, *J. Phys. D. Appl. Phys.* 51 (2018), 343001.
- [3] H.F. Renard, L. Johannes, P. Morsomme, Increasing diversity of biological membrane fission mechanisms, *Trends Cell Biol.* 28 (2018) 274–286.
- [4] Y. Caspi, C. Dekker, Divided we stand: splitting synthetic cells for their proliferation, *Syst. Synth. Biol.* 8 (2014) 249–269.
- [5] P. Schwille, J. Spatz, K. Landfester, E. Bodenschatz, S. Herminghaus, V. Sourjik, T. Erb, P. Bastiaens, R. Lipowsky, A. Hyman, P. Dabrock, J.-C. Baret, T. Vidakovic-Koch, P. Bieling, R. Dimova, H. Mutschler, T. Robinson, D. Tang, S. Wegner, K. Sundmacher, MaxSynBio: avenues towards creating cells from the bottom up, *Angew. Chem. Int. Ed.* 57 (2018) 13382–13392.
- [6] T. Trantidou, M.S. Friddin, A. Salehi-Reyhani, O. Ces, Y. Elani, Droplet microfluidics for the construction of compartmentalised model membranes, *Lab Chip* 18 (2018) 2488–2509.
- [7] P. Walde, K. Cosentino, H. Engel, P. Stano, Giant vesicles: preparations and applications, *ChemBioChem* 11 (2010) 848–865.
- [8] S.F. Fenz, K. Sengupta, Giant vesicles as cell models, *Integr. Biol.* 4 (2012) 982–995.
- [9] L.L. Jørgensen, G.C. Kemmer, T.G. Pomorski, Membrane protein reconstitution into giant unilamellar vesicles: a review on current techniques, *Eur. Biophys. J.* 46 (2017) 103–119.
- [10] R. Dimova, C. Marques, *The Giant Vesicle Book*, Taylor & Francis Group, LLC, Boca Raton, 2019.
- [11] R. Dimova, Giant vesicles and their use in assays for assessing membrane phase state, curvature, mechanics, and electrical properties, *Annu. Rev. Biophys.* 48 (2019) 93–119.
- [12] S. Deshpande, W.K. Spoelstra, M. van Doorn, J. Kerssemakers, C. Dekker, Mechanical division of cell-sized liposomes, *ACS Nano* 12 (2018) 2560–2568.
- [13] J. Steinkühler, S. Bartelt, S. Wegner, R.L. Knorr, R. Dimova, R. Lipowsky, Budding and fission of vesicles by control of membrane spontaneous curvature, *Biophys. J.* 116 (2019) 328a–329a.
- [14] W.T. Snead, C.C. Hayden, A.K. Gadok, C. Zhao, E.M. Lafer, P. Rangamani, J. C. Stachowiak, Membrane fission by protein crowding, *Proc. Natl. Acad. Sci.* 114 (2017) E3258.
- [15] T. Tanaka, R. Sano, Y. Yamashita, M. Yamazaki, Shape changes and Vesicle Fission of Giant Unilamellar Vesicles of Liquid-Ordered phase Membrane Induced by Lysophosphatidylcholine, *Langmuir* 20 (2004) 9526–9534.
- [16] Y. Inaoka, M. Yamazaki, Vesicle fission of giant unilamellar vesicles of liquid-ordered-phase membranes induced by amphiphiles with a single long hydrocarbon chain, *Langmuir* 23 (2007) 720–728.
- [17] P.F.F. Almeida, Thermodynamics of lipid interactions in complex bilayers, *Biochim. Biophys. Acta Biomembr.* 1788 (2009) 72–85.
- [18] S.P. Rayermann, G.E. Rayermann, C.E. Cornell, A.J. Merz, S.L. Keller, Hallmarks of reversible separation of living, unperturbed cell membranes into two liquid phases, *Biophys. J.* 113 (2017) 2425–2432.
- [19] A. Pralle, P. Keller, E.-L. Florin, K. Simons, J.K.H. Hörber, Sphingolipid-cholesterol rafts diffuse as small entities in the plasma membrane of mammalian cells, *J. Cell Biol.* 148 (2000) 997–1008.
- [20] D. Meder, M.J. Moreno, P. Verkade, W.L.C. Vaz, K. Simons, Phase coexistence and connectivity in the apical membrane of polarized epithelial cells, *Proc. Natl. Acad. Sci. U. S. A.* 103 (2006) 329–334.
- [21] R. Regmi, P.M. Winkler, V. Flauraud, K.J.E. Borgman, C. Manzo, J. Brugger, H. Rigneault, J. Wenger, M.F. García-Parajo, Planar optical nanoantennas resolve cholesterol-dependent nanoscale heterogeneities in the plasma membrane of living cells, *Nano Lett.* 17 (2017) 6295–6302.
- [22] C. Eggeling, C. Ringemann, R. Medda, G. Schwarzmann, K. Sandhoff, S. Polyakova, V.N. Belov, B. Hein, C. von Middendorff, A. Schönle, S.W. Hell, Direct observation of the nanoscale dynamics of membrane lipids in a living cell, *Nature* 457 (2009) 1159–U1121.
- [23] R. Yan, S. Moon, S.J. Kenny, K. Xu, Spectrally resolved and functional super-resolution microscopy via ultrahigh-throughput single-molecule spectroscopy, *Acc. Chem. Res.* 51 (2018) 697–705.
- [24] F.M. Göni, A. Alonso, F.X. Contreras, Membrane nanodomains, in: *eLS*, John Wiley & Sons, Ltd, 2020, pp. 1–8.
- [25] K. Simons, E. Ikonen, Functional rafts in cell membranes, *Nature* 387 (1997) 569–572.
- [26] D.A. Brown, E. London, Functions of lipid rafts in biological membranes, *Annu. Rev. Cell Dev. Biol.* 14 (1998) 111–136.
- [27] R. Lipowsky, Domain-induced budding of fluid membranes, *Biophys. J.* 64 (1993) 1133–1138.
- [28] F. Julicher, R. Lipowsky, Domain-induced budding of vesicles, *Phys. Rev. Lett.* 70 (1993) 2964–2967.
- [29] J.M. Allain, C. Storm, A. Roux, M.B. Amar, J.F. Joanny, Fission of a multiphase membrane tube, *Phys. Rev. Lett.* 93 (2004), 158104.
- [30] R. Lipowsky, R. Dimova, Domains in membranes and vesicles, *J. Phys. Condens. Matter* 15 (2003) S31–S45.
- [31] A. Roux, D. Cuvelier, P. Nassoy, J. Prost, P. Bassereau, B. Goud, Role of curvature and phase transition in lipid sorting and fission of membrane tubules, *EMBO J.* 24 (2005) 1537–1545.
- [32] M. Babst, D.J. Katzmann, W.B. Snyder, B. Wendland, S.D. Emr, Endosome-associated complex, ESCRT-II, recruits transport machinery for protein sorting at the multivesicular body, *Dev. Cell* 3 (2002) 283–289.
- [33] E. Morita, V. Sandrin, H.Y. Chung, S.G. Morham, S.P. Gygi, C.K. Rodesch, W. I. Sundquist, Human ESCRT and ALIX proteins interact with proteins of the midbody and function in cytokinesis, *EMBO J.* 26 (2007) 4215–4227.
- [34] N. Elia, R. Sougrat, T.A. Spurlin, J.H. Hurley, J. Lippincott-Schwartz, Dynamics of endosomal sorting complex required for transport (ESCRT) machinery during cytokinesis and its role in abscission, *Proc. Natl. Acad. Sci.* 108 (2011) 4846.
- [35] E. Morita, V. Sandrin, J. McCullough, A. Katsuyama, I. Baci Hamilton, W. I. Sundquist, ESCRT-III protein requirements for HIV-1 budding, *Cell Host Microbe* 9 (2011) 235–242.
- [36] M. Colombo, C. Moita, G. van Niel, J. Kowal, J. Vigneron, P. Benaroch, N. Manel, L.F. Moita, C. Théry, G. Raposo, Analysis of ESCRT functions in exosome biogenesis, composition and secretion highlights the heterogeneity of extracellular vesicles, *J. Cell Sci.* 126 (2013) 5553.
- [37] N. Loncle, M. Agromayor, J. Martin-Serrano, D.W. Williams, An ESCRT module is required for neuron pruning, *Sci. Rep.* 5 (2015) 8461.
- [38] J. Schöneberg, I.H. Lee, J.H. Iwasa, J.H. Hurley, Reverse-topology membrane scission by the ESCRT proteins, *Nat. Rev. Mol. Cell Biol.* 18 (2017) 5–17.
- [39] T. Kirchhausen, Three ways to make a vesicle, *Nat. Rev. Mol. Cell Biol.* 1 (2000) 187–198.
- [40] K.F. Leung, J.B. Dacks, M.C. Field, Evolution of the multivesicular body ESCRT machinery; retention across the eukaryotic lineage, *Traffic* 9 (2008) 1698–1716.
- [41] J. McCullough, A. Frost, W.I. Sundquist, Structures, functions, and dynamics of ESCRT-III/Vps4 membrane remodeling and fission complexes, *Annu. Rev. Cell Dev. Biol.* 34 (2018) 85–109.
- [42] Y. Avalos-Padilla, R.L. Knorr, R. Javier-Reyna, G. Garcia-Rivera, R. Lipowsky, R. Dimova, E. Orozco, The conserved ESCRT-III machinery participates in the phagocytosis of *Entamoeba histolytica*, *Front. Cell. Infect. Microbiol.* 8 (2018).
- [43] S. Banjade, S.G. Tang, Y.H. Shah, S.D. Emr, Electrostatic lateral interactions drive ESCRT-III heteropolymer assembly, *elife* 8 (2019).
- [44] 1423-3. Schöneberg, M.R. Pavlin, S. Yan, M. Righini, I.H. Lee, L.A. Carlson, A. H. Bahrami, D.H. Goldman, X.F. Ren, G. Hummer, C. Bustamante, J.H. Hurley, ATP-dependent force generation and membrane scission by ESCRT-III and Vps4, *Science* 362 (2018).
- [45] A. Booth, C.J. Marklew, B. Ciani, P.A. Beales, In vitro membrane remodeling by ESCRT is regulated by negative feedback from membrane tension, *iScience* 15 (2019) 173–184.
- [46] A. Zamborlini, Y. Usami, S.R. Radoshitzky, E. Popova, G. Palu, H. Göttlinger, Release of autoinhibition converts ESCRT-III components into potent inhibitors of HIV-1 budding, *Proc. Natl. Acad. Sci.* 103 (2006) 19140.
- [47] T. Muziol, E. Pineda-Molina, R.B. Ravelli, A. Zamborlini, Y. Usami, H. Göttlinger, W. Weissenhorn, Structural basis for budding by the ESCRT-III factor CHMP3, *Dev. Cell* 10 (2006) 821–830.
- [48] M. Bajorek, H.L. Schubert, J. McCullough, C. Langelier, D.M. Eckert, W.-M. B. Stubblefield, N.T. Uter, D.G. Myszkka, C.P. Hill, W.I. Sundquist, Structural basis for ESCRT-III protein autoinhibition, *Nat. Struct. Mol. Biol.* 16 (2009) 754–762.
- [49] L.-A. Carlson, Q.-T. Shen, Mark R. Pavlin, James H. Hurley, ESCRT filaments as spiral springs, *Dev. Cell* 35 (2015) 397–398.
- [50] L. Harker-Kirschneck, B. Baum, A.e., Saric, changes in ESCRT-III filament geometry drive membrane remodelling and fission in silico, *BMC Biol.* 17 (2019) 82.
- [51] M.A.Y. Adell, G.F. Vogel, M. Pakdel, M. Müller, H. Lindner, M.W. Hess, D. Teis, Coordinated binding of Vps4 to ESCRT-III drives membrane neck constriction during MVB vesicle formation, *J. Cell Biol.* 205 (2014) 33–49.
- [52] S. Tang, W.M. Henne, P.P. Borbat, N.J. Buchkovich, J.H. Freed, Y. Mao, J. C. Fromme, S.D. Emr, Structural basis for activation, assembly and membrane binding of ESCRT-III Snf7 filaments, *elife* 4 (2015), e12548.
- [53] J. McCullough, A.K. Clippinger, N. Talledge, M.L. Skowrya, M.G. Saunders, T. V. Naismith, L.A. Colf, P. Afonine, C. Arthur, W.I. Sundquist, P.I. Hanson, A. Frost, Structure and membrane remodeling activity of ESCRT-III helical polymers, *Science* 350 (2015) 1548.
- [54] N. Chiaruttini, L. Redondo-Morata, A. Colom, F. Humbert, M. Lenz, S. Scheuring, A. Roux, Relaxation of loaded ESCRT-III, *Cell* 163 (2015) 866–879.
- [55] B. Rozycki, E. Boura, J.H. Hurley, G. Hummer, Membrane-elasticity model of coatless vesicle budding induced by ESCRT complexes, *PLoS Comput. Biol.* 8 (2012).
- [56] E. Boura, V. Ivanov, L.A. Carlson, K. Mizuuchi, J.H. Hurley, Endosomal sorting complex required for transport (ESCRT) complexes induce phase-separated microdomains in supported lipid bilayers, *J. Biol. Chem.* 287 (2012) 28144–28151.
- [57] E.B. Frankel, R. Shankar, J.J. Moresco, J.R. Yates, N. Volkmann, A. Audhya, Ist1 regulates ESCRT-III assembly and function during multivesicular endosome biogenesis in *Caenorhabditis elegans* embryos, *Nat. Commun.* 8 (2017).
- [58] R.A. Buono, A. Leier, J. Paez-Valencia, J. Pennington, K. Goodman, N. Miller, P. Ahlquist, T.T. Marquez-Lago, M.S. Otegui, ESC RT-mediated vesicle concatenation in plant endosomes, *J. Cell Biol.* 216 (2017) 2167–2177.
- [59] E.M. Wenzel, S.W. Schultz, K.O. Schink, N.M. Pedersen, V. Nahse, A. Carlson, A. Brech, H. Stenmark, C. Raiborg, Concerted ESCRT and clathrin recruitment waves define the timing and morphology of intraluminal vesicle formation, *Nat. Commun.* 9 (2018).

- [60] S.L. Veatch, S.L. Keller, Seeing spots: complex phase behavior in simple membranes, *Biochim. Biophys. Acta, Mol. Cell Res.* 1746 (2005) 172–185.
- [61] M.C. Blosser, C.E. Cornell, S.P. Rayermann, S.L. Keller, Phase diagrams and tie lines in giant unilamellar vesicles, in: R. Dimova, C. Marques (Eds.), *The Giant Vesicle Book*, Taylor & Francis Group LLC, Boca Raton, 2019.
- [62] T. Wollert, J.H. Hurley, Molecular mechanism of multivesicular body biogenesis by ESCRT complexes, *Nature* 464 (2010) 864–U873.
- [63] W.M. Henne, N.J. Buchkovich, Y.Y. Zhao, S.D. Emr, The endosomal sorting complex ESCRT-II mediates the assembly and architecture of ESCRT-III helices, *Cell* 151 (2012) 356–371.
- [64] C. Dietrich, L.A. Bagatolli, Z.N. Volovyk, N.L. Thompson, M. Levi, K. Jacobson, E. Gratton, Lipid rafts reconstituted in model membranes, *Biophys. J.* 80 (2001) 1417–1428.
- [65] S.L. Veatch, S.L. Keller, Separation of liquid phases in giant vesicles of ternary mixtures of phospholipids and cholesterol, *Biophys. J.* 85 (2003) 3074–3083.
- [66] N. Bezlyepkina, R.S. Gracia, P. Shchelokovskyy, R. Lipowsky, R. Dimova, Phase diagram and tie-line determination for the ternary mixture DOPC/eSM/cholesterol, *Biophys. J.* 104 (2013) 1456–1464.
- [67] M.C. Blosser, C.E. Cornell, S.P. Rayermann, S.L. Keller, Phase diagrams and tie lines in giant unilamellar vesicles, in: R. Dimova, C. Marques (Eds.), *The Giant Vesicle Book*, Taylor & Francis Group LLC, Boca Raton, 2019, pp. 401–416.
- [68] K. Simons, W.L.C. Vaz, Model systems, lipid rafts, and cell membranes, *Annual Review of Biophysics and Biomolecular Structure* 33 (2004) 269–295.
- [69] N. Kahya, Protein–protein and protein–lipid interactions in domain-assembly: lessons from giant unilamellar vesicles, *Biochim. Biophys. Acta Biomembr.* 1798 (2010) 1392–1398.
- [70] E. Sezgin, H.J. Kaiser, T. Baumgart, P. Schwillie, K. Simons, I. Levental, Elucidating membrane structure and protein behavior using giant plasma membrane vesicles, *Nat. Protoc.* 7 (2012) 1042–1051.
- [71] J. Hjort Ipsen, G. Karlström, O.G. Mourtsen, H. Wennerström, M.J. Zuckermann, Phase equilibria in the phosphatidylcholine-cholesterol system, *Biochim. Biophys. Acta Biomembr.* 905 (1987) 162–172.
- [72] E. Sezgin, I. Levental, S. Mayor, C. Eggeling, The mystery of membrane organization: composition, regulation and roles of lipid rafts, *Nat. Rev. Mol. Cell Biol.* 18 (2017) 361–374.
- [73] S.L. Veatch, S.L. Keller, A closer look at the canonical &raft mixture' in model membrane studies, *Biophys. J.* 84 (2003) 725–726.
- [74] T.Y. Wang, R. Leventis, J.R. Silvius, Fluorescence evaluation of molecular partitioning into lipid &rafts' (liquid-ordered domains) in lipid model membranes, *Mol. Biol. Cell* 11 (2000) 4a–5a.
- [75] D. Lingwood, K. Simons, Lipid rafts as a membrane-organizing principle, *Science* 327 (2010) 46–50.
- [76] S. Patarraia, Y.G. Liu, R. Lipowsky, R. Dimova, Effect of cytochrome c on the phase behavior of charged multicomponent lipid membranes, *BBA-Biomembranes* 2014 (1838) 2036–2045.
- [77] S.T. Huber, S. Mostafavi, S.A. Mortensen, C. Sachse, Structure and assembly of ESCRT-III helical Vps24 filaments, *Sci. Adv.* 6 (2020), eaba4897.
- [78] Y. Avalos-Padilla, A. Betanzos, R. Javier-Reyna, G. García-Rivera, B. Chávez-Munguía, A. Lagunes-Guillén, J. Ortega, E. Orozco, EhVps32 is a vacuole-associated protein involved in pinocytosis and phagocytosis of entamoeba histolytica, *PLoS Pathog.* 11 (2015), e1005079.
- [79] G. MacBeath, Protein microarrays and proteomics, *Nat. Genet.* 32 (2002) 526–532.
- [80] T. Kodadek, Protein microarrays: prospects and problems, *Chem. Biol.* 8 (2001) 105–115.
- [81] Y.S. Sun, J.P. Landry, Y.Y. Fei, X.D. Zhu, J.T. Luo, X.B. Wang, K.S. Lam, Effect of fluorescently labeling protein probes on kinetics of protein-ligand reactions, *Langmuir* 24 (2008) 13399–13405.
- [82] A.G. Ayuyan, F.S. Cohen, Lipid peroxides promote large rafts: effects of excitation of probes in fluorescence microscopy and electrochemical reactions during vesicle formation, *Biophys. J.* 91 (2006) 2172–2183.
- [83] J. Zhao, J. Wu, H.L. Shao, F. Kong, N. Jain, G. Hunt, G. Feigenson, Phase studies of model biomembranes: Macroscopic coexistence of L alpha plus L beta, with light-induced coexistence of L alpha plus L o Phases, *Biochim. Biophys. Acta Biomembr.* 1768 (2007) 2777–2786.
- [84] M.I. Angelova, D.S. Dimitrov, Liposome Electroformation, *Faraday Discuss.* 81 (1986), 303.
- [85] N. Yandrapalli, T. Robinson, Ultra-high capacity microfluidic trapping of giant vesicles for high-throughput membrane studies, *Lab Chip* 19 (2019) 626–633.
- [86] R. Lipowsky, Budding of membranes induced by intramembrane domains, *J. Phys. II* 2 (1992) 1825–1840.
- [87] C.C. Vequi-Suplicy, K.A. Riske, R.L. Knorr, R. Dimova, Vesicles with charged domains, *BBA-Biomembranes* 1798 (2010) 1338–1347.
- [88] M. Alqabandi, N. de Franceschi, S. Maity, N. Miguet, M. Bally, W.H. Roos, W. Weissenhorn, P. Bassereau, S. Manganot, The ESCRT-III isoforms CHMP2A and CHMP2B display different effects on membranes upon polymerization, *BMC Biol.* 19 (2021) 66.
- [89] I.-H. Lee, H. Kai, L.-A. Carlson, J.T. Groves, J.H. Hurley, Negative membrane curvature catalyzes nucleation of endosomal sorting complex required for transport (ESCRT)-III assembly, *Proc. Natl. Acad. Sci.* 112 (2015) 15892.
- [90] A. Bertin, N. de Franceschi, E. de la Mora, S. Maiti, M. Alqabandi, N. Miguet, A. di Cicco, W.H. Roos, S. Manganot, W. Weissenhorn, P. Bassereau, Human ESCRT-III polymers assemble on positively curved membranes and induce helical membrane tube formation, *Nat. Commun.* 11 (2020) 2663.
- [91] B. Kubsch, T. Robinson, R. Lipowsky, R. Dimova, Solution asymmetry and salt expand fluid-fluid coexistence regions of charged membranes, *Biophys. J.* 110 (2016) 2581–2584.
- [92] B. Kubsch, T. Robinson, J. Steinkühler, R. Dimova, Phase behavior of charged vesicles under symmetric and asymmetric solution conditions monitored with fluorescence microscopy, *J. Vis. Exp.* 128 (2017), e56034.
- [93] T. Baumgart, G. Hunt, E.R. Farkas, W.W. Webb, G.W. Feigenson, Fluorescence probe partitioning between L-o/L-d phases in lipid membranes, *BBA-Biomembranes* 1768 (2007) 2182–2194.
- [94] C.K. Haluska, A.P. Schroder, P. Didier, D. Heissler, G. Dupontail, Y. Mely, C. M. Marques, Combining fluorescence lifetime and polarization microscopy to discriminate phase separated domains in giant unilamellar vesicles, *Biophys. J.* 95 (2008) 5737–5747.
- [95] G.G. Putzel, M. Schick, Insights on raft behavior from minimal phenomenological models, *J. Phys. Condens. Mater* 23 (2011).
- [96] M. Heinrich, A. Tian, C. Esposito, T. Baumgart, Dynamic sorting of lipids and proteins in membrane tubes with a moving phase boundary, *Proc. Natl. Acad. Sci. U. S. A.* 107 (2010) 7208–7213.
- [97] S. Semrau, T. Idema, L. Holtzer, T. Schmidt, C. Storm, Accurate determination of elastic parameters for multicomponent membranes, *Phys. Rev. Lett.* 100 (2008).
- [98] M. Karimi, J. Steinkühler, D. Roy, R. Dasgupta, R. Lipowsky, R. Dimova, Asymmetric ionic conditions generate large membrane curvatures, *Nano Lett.* 18 (2018) 7816–7821.
- [99] T. Bhatia, T. Robinson, R. Dimova, Membrane permeability to water measured by microfluidic trapping of giant vesicles, *Soft Matter* 16 (2020) 7359–7369.
- [100] M.A.Y. Adell, S.M. Migliano, S. Upadhyayula, Y.S. Bykov, S. Sprenger, M. Pakdel, G.F. Vogel, G. Jih, W. Skillern, R. Behrouzi, M. Babst, O. Schmidt, M.W. Hess, J.A. G. Briggs, T. Kirchhausen, D. Teis, Recruitment dynamics of ESCRT-III and Vps4 to endosomes and implications for reverse membrane budding, *elife* 6 (2017).
- [101] V. Mercier, J. Larios, G. Molinard, A. Goujon, S. Matile, J. Gruenberg, A. Roux, Endosomal membrane tension regulates ESCRT-III-dependent intra-luminal vesicle formation, *Nat. Cell Biol.* 22 (2020) 947–959.
- [102] Y.J. Im, T. Wollert, E. Boura, J.H. Hurley, Structure and function of the ESCRT-II-III interface in multivesicular body biogenesis, *Dev. Cell* 17 (2009) 234–243.
- [103] A. Audhya, A. Schuh, J. Mayers, I. Fyfe, M. Edwardson, Mechanisms of ESCRT-mediated cargo sorting and degradation, *FASEB J.* 26 (2012).
- [104] J. Steinkühler, P. De Tillieux, R.L. Knorr, R. Lipowsky, R. Dimova, Charged giant unilamellar vesicles prepared by electroformation exhibit nanotubes and transbilayer lipid asymmetry, *Sci. Rep.* 8 (2018) 11838.
- [105] G. Fabrikant, S. Lata, J.D. Richez, J.A.G. Briggs, W. Weissenhorn, M.M. Kozlov, Computational model of membrane fission catalyzed by ESCRT-III, *PLoS Comput. Biol.* 5 (2009).
- [106] J. Moser von Filseck, L. Barberi, N. Talledge, I.E. Johnson, A. Frost, M. Lenz, A. Roux, Anisotropic ESCRT-III architecture governs helical membrane tube formation, *Nat. Commun.* 11 (2020) 1516.
- [107] L. Miao, U. Seifert, M. Wortis, H.G. Dobreiner, Budding transitions of fluid-bilayer vesicles - the effect of area-difference elasticity, *Phys. Rev. E* 49 (1994) 5389–5407.
- [108] N.-N. Deng, M. Yelleswarapu, L. Zheng, W.T.S. Huck, Microfluidic assembly of monodisperse vesosomes as artificial cell models, *J. Am. Chem. Soc.* 139 (2017) 587–590.
- [109] M. Weiss, J.P. Frohnmayer, L.T. Benk, B. Haller, J.-W. Janiesch, T. Heitkamp, M. Borsch, R.B. Lira, R. Dimova, R. Lipowsky, E. Bodenschatz, J.-C. Baret, T. Vidakovic-Koch, K. Sundmacher, I. Platzman, J.P. Spatz, Sequential bottom-up assembly of mechanically stabilized synthetic cells by microfluidics, *Nat. Mater.* 17 (2018) 89–96.
- [110] S. Li, X. Wang, W. Mu, X. Han, Chemical signal communication between two protoorganelles in a lipid-based artificial cell, *Anal. Chem.* 91 (2019) 6859–6864.
- [111] K. Göpfrich, B. Haller, O. Stauer, Y. Dreher, U. Mersdorf, I. Platzman, J.P. Spatz, One-pot assembly of complex giant unilamellar vesicle-based synthetic cells, *ACS Synth. Biol.* 8 (2019) 937–947.

Supporting information

ESCRT-III induces phase separation in model membranes prior to budding and causes invagination of the liquid-ordered phase

Yunuen Avalos-Padilla,^{1,2,3*} Vasil. N. Georgiev¹ and Rumiana Dimova^{1*}

¹ Department of Theory and Bio-Systems, Max Planck Institute of Colloids and Interfaces, Science Park Golm, 14424 Potsdam, Germany

² Nanomalaria Group, Institute for Bioengineering of Catalonia (IBEC), The Barcelona Institute of Science and Technology, Baldori Reixac 10-12, ES-08028 Barcelona, Spain

³ Present address: Barcelona Institute for Global Health (ISGlobal, Hospital Clínic-Universitat de Barcelona), Rosselló 149-153, ES-08036 Barcelona, Spain

* Correspondence:

Dr. Rumiana Dimova
Rumiana.Dimova@mpikg.mpg.de

Dr. Yunuen Avalos-Padilla
yavalos@ibecbarcelona.eu

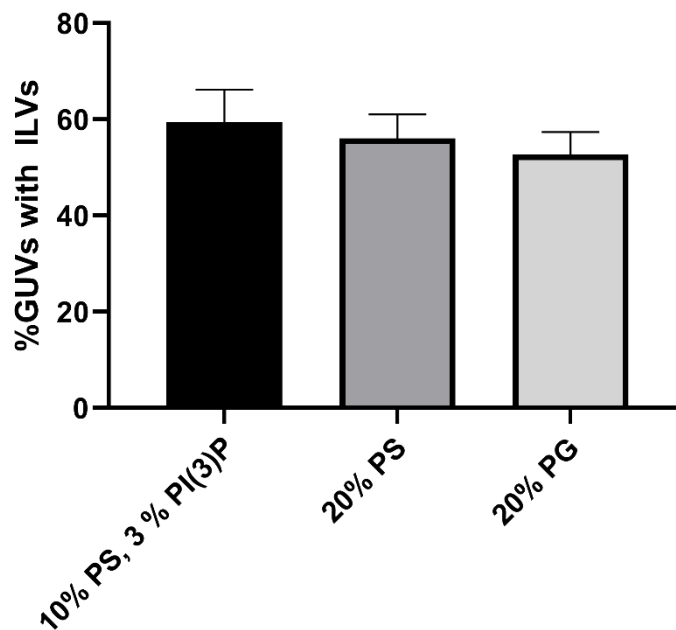


Figure S1. GUVs prepared with a mixture of different negatively charged lipids, POPG:POPS:PI(3)P (87:10:3); POPC:POPS (80:20) and POPC:POPG (80:20) (negative charge molar ratio of ~20%) and labelled with 0.1 mol% of DiI_{C18} were incubated with 125 nM EhVps20t, 600 nM EhVps32 and 200 nM EhVps24 and the number of GUVs with at least 4 ILVs were counted in a total of 50 vesicles. Bars represent the mean and standard error of three independent experiments.

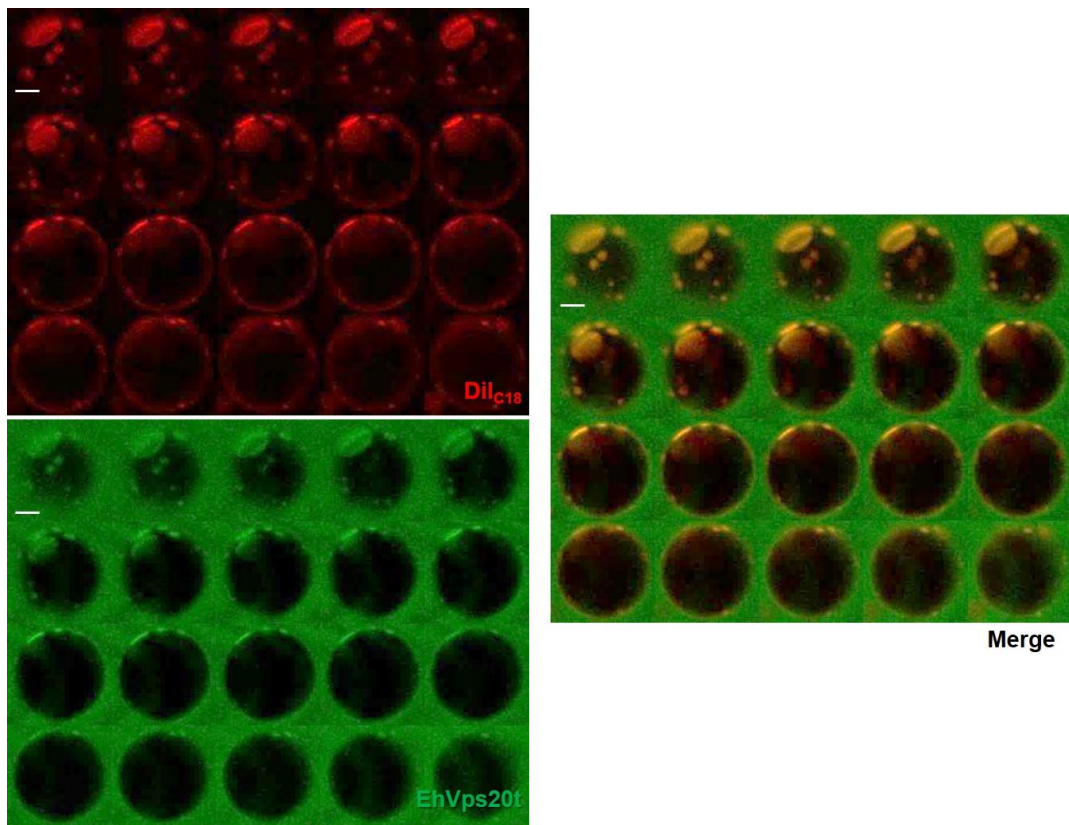


Figure S2. Confocal xy cross-sections (20 in total) at different heights across the upper half of the vesicle shown in Fig. 2 in the main text. The GUV is with homogeneous lipid composition (DOPG:eSM:Chol 10:65:25, and 0.3 mol% DiI_{C18}, false color red) and exhibits domains after 10 min incubation at room temperature with 125 nM of a mixture of 1:4 labelled:unlabelled EhVps20t, false color green, and 600 nM EhVps32. Scale bars correspond to 10 μ m.

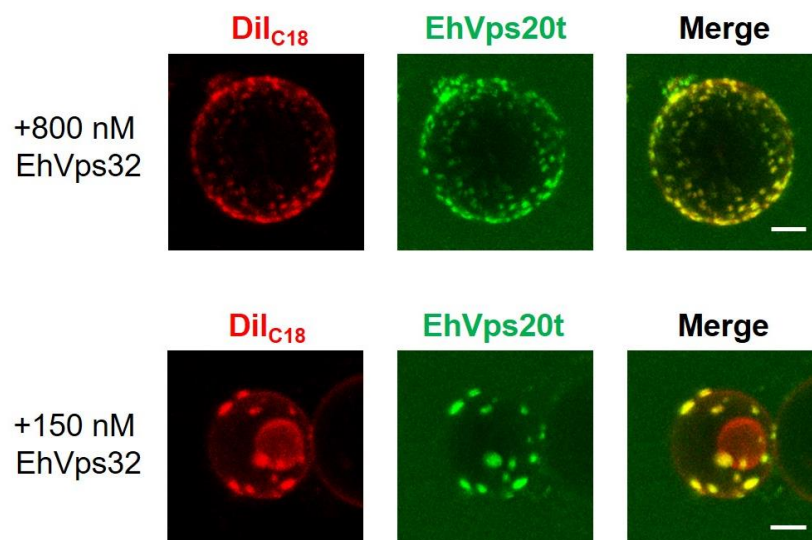


Figure S3. Images of two GUV with homogeneous lipid composition (DOPG:eSM:Chol 10:65:25, and 0.3 mol% DiI_{C18}, false color red), which exhibit small domains shortly (couple of minutes) after incubation at room temperature with 125 nM EhVps20t (mixture of 1:4 labelled:unlabelled, false color green), and either 800 nM or 150 nM of EhVps32 as indicated on the left. Over time the domains coarsen. The red circular object in the GUV in the bottom row is a

smaller vesicle initially present before the addition of the proteins. Scale bars corresponds to 10 μm .

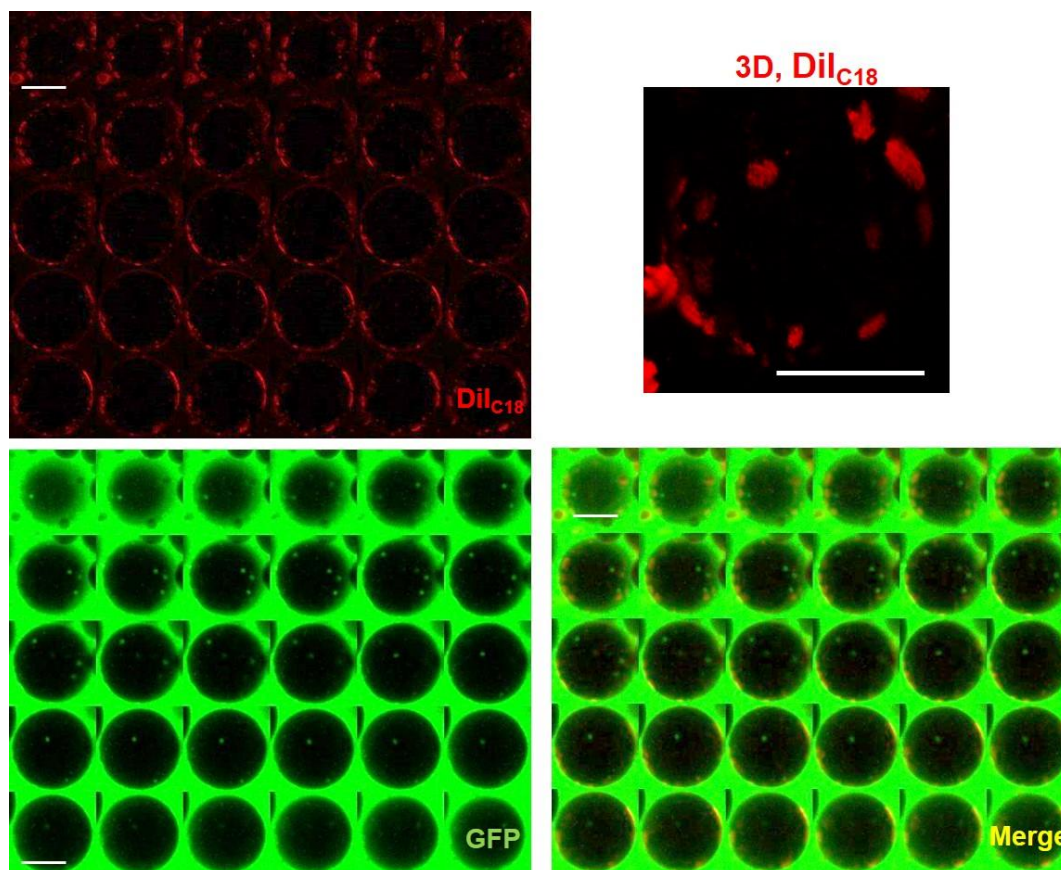


Figure S4. Confocal xy cross-sections (membrane dye DiI_{C18}, GFP and merged signal; images enhanced) at different heights across the lower half of the vesicle shown in Fig. 3 in the main text and 3D reconstruction of the total projection of the red channel showing the Ld membrane domains on the surface of the same GUV. Several intraluminal vesicles are seen in the GFP and merged images at different height as little green spots inside the GUV. The scale bars correspond to 20 μm .

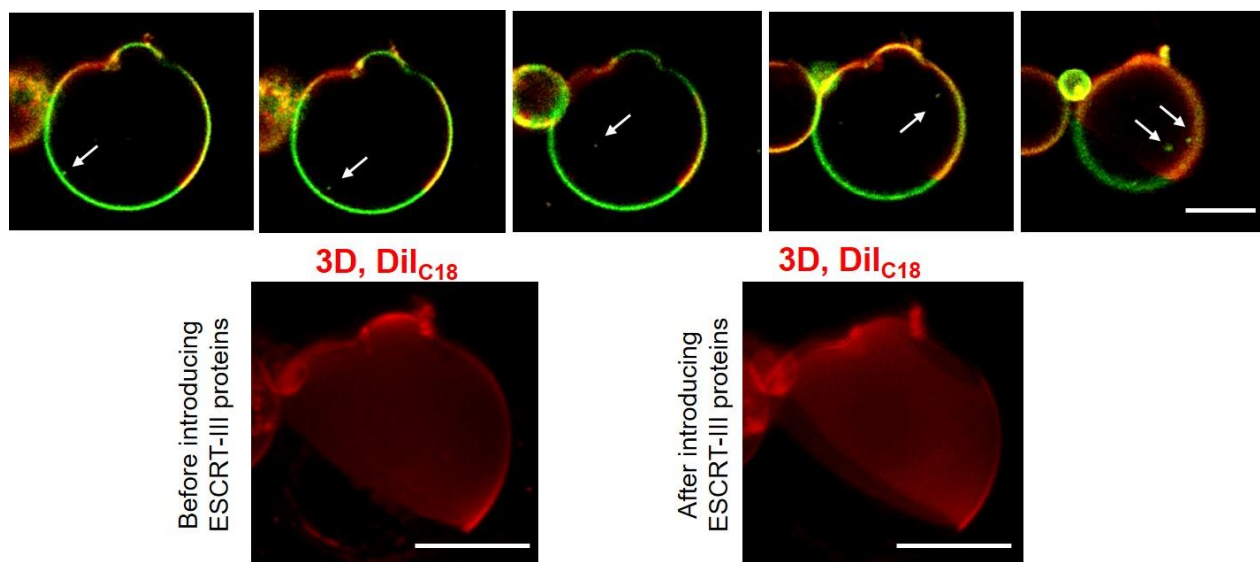


Figure S5. Confocal xy cross-sections (merged signal, upper row) and 3D reconstruction of the total projection of the red channel (lower row) of the vesicle in Fig. 4 in the main text showing different ILVs (seen as small green spots, arrows) located in the vesicle interior. The 3D projections show the Ld membrane domains on the surface of the GUV before and after EhVps20t, EhVps32 and EhVps24 addition. The vesicle appears deformed because it is pressed against the microfluidic posts. The red signal in the upper right part of the vesicle close to the microfluidic post is from a smaller vesicle which has ruptured prior to trapping the GUV. The GUV composition is DOPG:eSM:Chol 20:49:30, 0.3 mol% DiI_{C18} (false color red) and 0.75 mol% DSPE-PEG2000-CF (false color green). Scale bars correspond to 20 μ m. See also Movie S2.